LBNL-TBD

Mobility of Tritium in Engineered and Earth Materials at the NuMI Facility, Fermilab

Phase II: Final Report

Investigators:

Quanlin Zhou, Stefan Finsterle,
Lehua Pan and Yingqi Zhang

Earth Sciences Division
Lawrence Berkeley National Laboratory (LBNL)
Berkeley, California

March 12, 2010

This work was supported by the Fermi National Accelerator Laboratory (Fermilab). The support is provided to Berkeley Lab through the U.S. Department of Energy Contract No. DE-AC02-05CH11231.

DISCLAIMER

This document was prepared as an account of work sponsored by the United States Government. While this document is believed to contain correct information, neither the United States Government nor any agency thereof, nor The Regents of the University of California, nor any of their employees, makes any warranty, express or implied, or assumes any legal responsibility for the accuracy, completeness, or usefulness of any information, apparatus, product, or process disclosed, or represents that its use would not infringe privately owned rights. Reference herein to any specific commercial product, process, or service by its trade name, trademark, manufacturer, or otherwise, does not necessarily constitute or imply its endorsement, recommendation, or favoring by the United States Government or any agency thereof, or The Regents of the University of California. The views and opinions of authors expressed herein do not necessarily state or reflect those of the United States Government or any agency thereof, or The Regents of the University of California.

Ernest Orlando Lawrence Berkeley National Laboratory
is an equal opportunity employer

TABLE OF CONTENTS

LIST OF FIGURES ii
LIST OF TABLES iii
EXECUTIVE SUMMARY iv
1. INTRODUCTION 1
1.1 Background 1
1.2 Goal 2
1.3 Phase I Studies 2
1.4 Phase II Objectives 3
1.5 Approach 4
2. Measurements of flow and transport 5
2.1 Flow Measurements 5
2.2 Concentration Measurements 7
3. NUMERICAL MODEL DEVELOPMENT 9
3.1 Model Domain 9
3.2 Mesh Generation 10
3.3 Material Properties 13
3.4 Initial and Boundary Conditions 15
3.5 Steady-State Simulation and Comparison to Flow Data 15
3.6 Tritium Transport Simulation and Prediction 18
4. SUMMARY AND CONCLUSIONS 20
5. ACKNOWLEDGMENT 20
6. REFERENCES 21

LIST OF FIGURES

Figure 1. Schematic of the NuMI facility (not to scale; modified from Hylen, 2006a, Slide 1).. 1

Figure 2. Schematic of the general layout of the NuMI facility, and key processes affecting transport of tritium ('T' indicates "tritiated"; red thick arrows indicate ventilation direction; red thin arrows indicate particle beam and radiation). (A) Pre-Target Tunnel: Tritium enters this section of the NuMI either in the water collected as seepage, or as water vapor leaking from the Target Hall. (B) Target Pile and Target Hall: Tritium produced around the target is transported within the Target Hall as water vapor; it condenses, is absorbed, or is transported in vapor or liquid form to other locations in the facility. (C) Decay Pipe and passageway: Tritium vapor ventilated along the passageway partitions into water seeping along the walls, which is collected through grates by the main drain. Tritium produced in the fractured rock diffuses from the matrix to the fractures, where it is carried by water to the drainage system (dimple mat and main drain). Tritium produced in the Decay Pipe concrete may diffuse to the dimple mat. (D) Absorber Hall: Tritium produced by the absorbers is transported in vapor form along the passageway, and in liquid form to the main drain. 3

Figure 3. Tritium concentration in the sump water collected in the holding tank and beam intensity, and converted tritium mass using the flow rate of 157 gpm. 8

Figure 4. Base mesh at Section B: gridblock centers are shown as green dots; gridblock interfaces are in black lines. Three zones are roughly defined based on the flow conditions, materials, and underground objects: convergent flow zone (area between the outer red and blue circle), tritium production zone within rock (area between the blue and the middle red circles), decay tunnel zone backfilled with concrete (area between the two inner red circles), as well as the walkway and vacuum pipe. 9

Figure 5. Representative cross sections B through M, with focus on the area for mesh deformation. The green symbols in Section B 2D mesh represent gridblocks for the base section, with gridblock interfaces in black lines. The red points (within concrete) and purple points (within walkway) are anchor points with known coordinate shifts (displacement in both X and Y directions). The interface-intersection points along the blue circle are fixed for all sections with zero shifts, while the innermost red circle (vacuum pipe) is a rigid body with horizontal shifts only. Only the portion of the mesh in the area between the blue circle and the innermost red circle is distorted. ... 11

Figure 6. Tritium mass remaining in the concrete as a function of (a) intrinsic permeability with high water saturation, and (b) water saturation with the measured intrinsic permeability of concrete. Also shown in (b) are saturation-dependent tritium mass generated and decayed in concrete pore water, as well as the mass released from concrete pore water to the drainage system. 16

Figure 7. Beam intensity (POT/year) for the low-energy experiments from 2006 to 2013 and the high-energy experiments from 2014 to 2020. The corresponding tritium generation rates in the concrete assume fully water saturated conditions. 18

Figure 8. Cumulative activity of tritium generated and contained in the concrete pore water, and released into the drainage system during and after beam operation 19

LIST OF TABLES

Table 1. Measured rates of flow seeping into the excavated NuMI tunnel from different facility components in 2001 and 2002, as well as the calculated flow rates for the entire system 6

Table 2. Measured rates of flow seeping into the excavated NuMI tunnel from different facility components in 2001 and 2002, as well as the calculated flow rates for the entire system 7

Table 3. Hydraulic and transport parameters used in the flow and transport model 14

EXECUTIVE SUMMARY

Background

This report summarizes the Phase II work done between March 2007 and November, 2009 by Lawrence Berkeley National Laboratory (LBNL) scientists to assist Fermi National Accelerator Laboratory (Fermilab) staff in understanding tritium transport at the Neutrino at the Main Injector (NuMI) facility.

As a byproduct of beamline operation, the facility produces (among other radionuclides) tritium in engineered materials and the surrounding rock formation. Once the tritium is generated, it may be contained at the source location, migrate to other regions within the facility, or be released to the surrounding environment.

The main issue that prompted Fermilab to seek LBNL's assistance in understanding tritium transport at the NuMI facility was the observation that tritium levels in collected drainage water showed only a modest decline after the beam was turned off in February 2006. This behavior was unexpected and raised the question of where the tritium was coming from, and how it made its way into air and water collected along the facility. An understanding of tritium behavior in engineered and earth materials as well as through underground openings is needed to address key environmental concerns about possible tritium levels when the beamline is operated for longer durations and/or at higher intensities.

Phase I of this project focused on data analysis and interpretation for conceptual model development, literature review on tritium migration, laboratory experiments for the determination of tritium diffusion coefficients, and preliminary predictive modeling using a representative, two-dimensional cross section. This work is documented in Finsterle et al. (2007).

Phase II of this project focused on the development and calibration of a three-dimensional model of the decay-pipe region and surrounding formation. Using actual and proposed beam operation and associated tritium production rates, the model is then used to examine factors affecting tritium migration during and after beam operation.

1. INTRODUCTION

1.1 Background

Fermi National Accelerator Laboratory (Fermilab) operates the Neutrino at the Main Injector (NuMI) beamline for experimental studies in physics. NuMI is an approximately 1,300 m long underground facility, consisting of a Pre-Target Tunnel, the Target Pile within the Target Hall, the Decay Pipe, a passageway running parallel to the Decay Pipe, the Absorber Hall, the MINOS Hall, several ventilation shafts, and various surface facilities (Figure 1). The slope of the Decay Pipe is approximately 5.8%; the depth of the sump is approximately 100 m below land surface. The facility has been excavated in Silurian dolomite, siltstone and shale overlain by glacial till. Airflow through NuMI is controlled by two engineered ventilation systems, and the exhaust air is discharged to the atmosphere at four locations. Water entering the facility is collected in a drainage system and pumped to surface holding tanks.

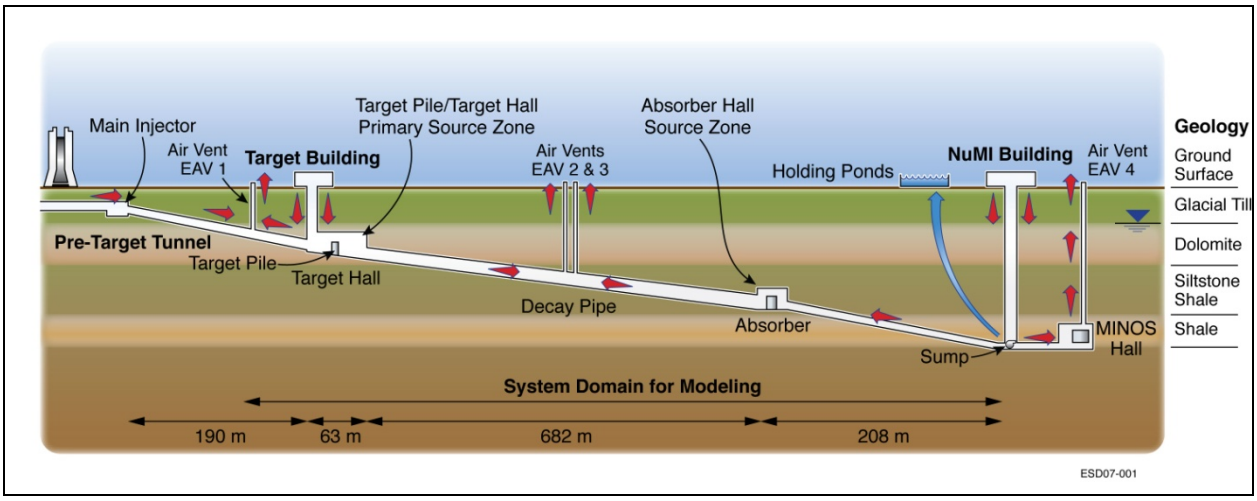

Figure 1. Schematic of the NuMI facility (not to scale; modified from Hylen, 2006a, Slide 1)

The NuMI beamline produces (among other radionuclides) tritium as a byproduct. This tritium production occurs predominantly in the Target Pile within the Target Hall, but also in the Absorber Hall, in the concrete along the Decay Pipe, and in the surrounding rock formation. Tritium may be generated in the gas phase, in pore-water, and in the solid components of the surrounding engineered and earth materials. Once the tritium is generated, it may be contained at the source location or migrate to other parts of the facility, with the possibility of being released to the surrounding environment. To monitor the fate of tritium, samples of water, concrete, and rock have been collected at multiple locations within the facility to infer tritium concentrations in the vapor phase, pore-water, drainage water, condensate, and solid materials. Preliminary analyses of the data show that tritium concentrations in drainage water pumped from the facility (while meeting environmental standards) remain on the order of 10 pCi/mL when the NuMI beamline is turned off, which is about a factor of two lower than the concentrations observed during beam operation. This suggests that the tritium generated in engineered and earth materials during beam operation is slowly released from the source zones and transported to the Decay

Pipe region through relatively mobile phases (e.g., ventilation air, collected water, and groundwater).

1.2 Goal

The overall goal of this project is to better understand the fate of tritium in the NuMI facility, in order to (1) evaluate potential environmental impacts, (2) determine tritium sources after the beam is shut off, (3) estimate the effects of the planned increase in beam intensity on tritium production and tritium releases, and (4) help design and optimize mitigation measures.

1.3 Phase I Studies

Phase I of this project was conducted between June 13 and September 30, 2006 and is documented in a progress report (Finsterle et al., 2007). The main purpose of this initial work phase was to develop a conceptual understanding of tritium inventory as well as tritium migration mechanisms and pathways. This conceptual understanding of tritium production and transport in the NuMI facility was developed based on a systematic analysis of Fermilab's tritium data as well as preliminary laboratory and modeling work. The main tritium transport mechanisms identified are (1) advective transport with airflow and mass transfer between gaseous and aqueous phases in the passageway (also referred to as walkway) and other underground openings, (2) advective and diffusive transport in concrete and fractured rock, and (3) mass transfer between tritium vapor in the underground openings and concrete or rock walls.

The conceptual model is sketched in Figure 2, which shows the main components of the NuMI facility as well as the key processes contributing to tritium production, fate, and transport through underground openings as well as engineered and earth materials.

The conceptual model was based on tritium concentration measurements at different locations within the facility. These data were supplemented with literature information and measurements of diffusion coefficients, and analyzed by considering operational conditions (i.e., beam operation, ventilation regime, installation of dehumidifiers, drainage system layout, etc.) in the facility.

A simplified numerical model (a vertical cross section of the decay pipe) was developed to integrate hypothesized processes and features as well as geometry elements into a tritium fate and transport model of the NuMI facility. The aim was to reproduce the observed system behavior and to simulate tritium transport from three different sources (fractured rock, concrete, and passageway). It was determined that the dominant tritium contribution to drainage water appeared to be from the airflow through the passageway, which contained high tritium concentrations. The preliminary simulations indicate that contributions from tritium sources in the fractured rock and concrete were not significant. Tritium continued to be released to the main drain from the fractured rock, the concrete, from vapor flow through the passageway (during ventilation), and back-diffusion from the concrete to the passageway (when ventilation was off).

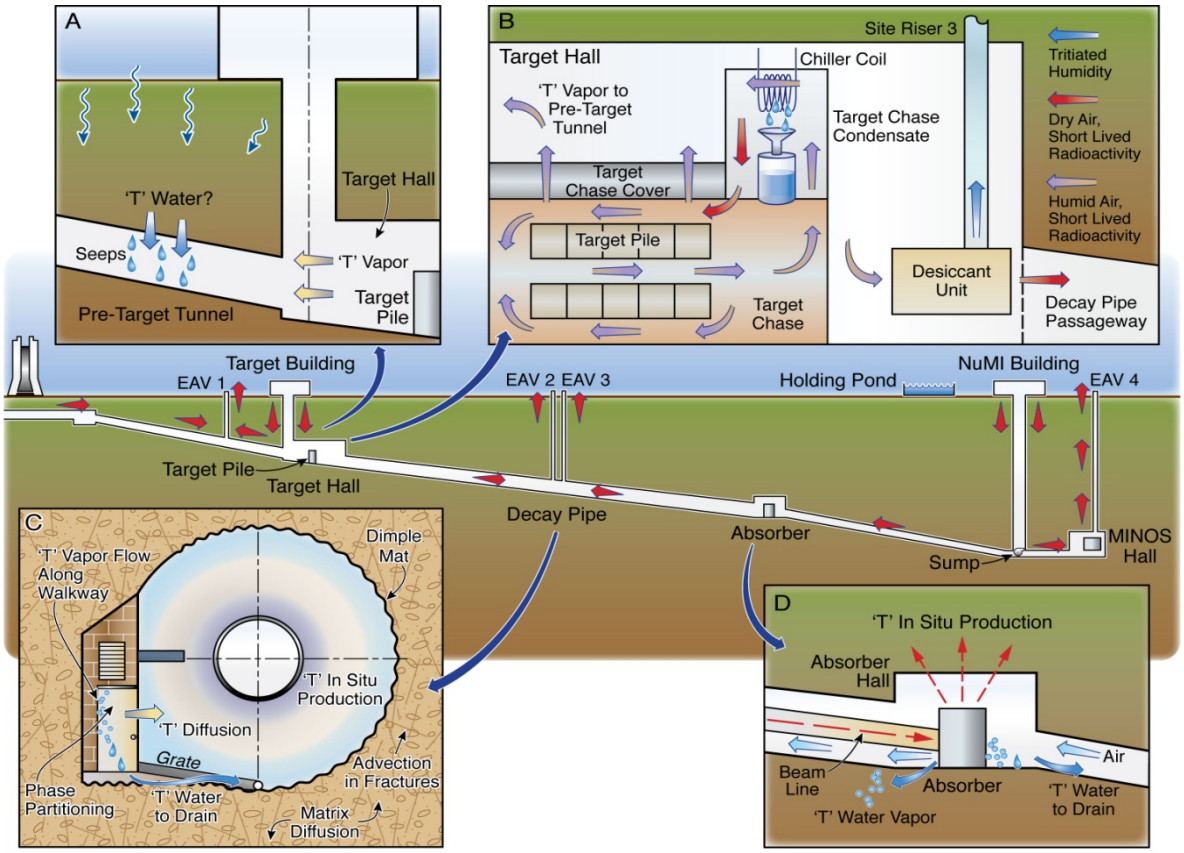

Figure 2. Schematic of the general layout of the NuMI facility, and key processes affecting transport of tritium ('T' indicates "tritiated"; red thick arrows indicate ventilation direction; red thin arrows indicate particle beam and radiation). (A) Pre-Target Tunnel: Tritium enters this section of the NuMI either in the water collected as seepage, or as water vapor leaking from the Target Hall. (B) Target Pile and Target Hall: Tritium produced around the target is transported within the Target Hall as water vapor; it condenses, is absorbed, or is transported in vapor or liquid form to other locations in the facility. (C) Decay Pipe and passageway: Tritium vapor ventilated along the passageway partitions into water seeping along the walls, which is collected through grates by the main drain. Tritium produced in the fractured rock diffuses from the matrix to the fractures, where it is carried by water to the drainage system (dimple mat and main drain). Tritium produced in the Decay Pipe concrete may diffuse to the dimple mat. (D) Absorber Hall: Tritium produced by the absorbers is transported in vapor form along the passageway, and in liquid form to the main drain.

1.4 Phase II Objectives

The purpose of Phase II of this project is to develop predictive models for tritium transport during and after beam operation, accounting for liquid, vapor, air, and tritium transport in concrete, fractured rock, and underground openings.

1.5 Approach

A full-scale, three-dimensional numerical model of the decay pipe region is developed, accounting for liquid, vapor, air, and tritium transport in concrete, fractured rock, and underground openings. The model uses an approximate representation of the stratigraphy. Confidence in the model is gained by comparison between the calculated and measured water flow in the main drain as well as calculated and measured tritium concentrations. No formal calibration is performed, i.e., no attempt is made to accurately reproduce past operating conditions and to quantitatively match the corresponding observed system response. Certain processes (e.g., solid diffusion) are represented by simplified approaches using effective parameters. Parameters are taken from the literature or determined through simple laboratory experiments. Time-dependent and spatially variable tritium generation rates as well as operational conditions (including ventilation rates and tritium vapor concentrations at upstream and downstream ends of the passageway) are provided by Fermilab. The evolution of the tritium plume is simulated for the production period (approximately 14 years). A limited sensitivity analysis involving key parameters is performed.

2. MEASUREMENTS OF FLOW AND TRANSPORT

Observations of flow and transport variables have been taken by Fermilab to understand the response of the NuMI facility system to the induced transient fluid flow and tritium transport. Some of the flow and transport measurements were summarized in the Phase I project report (Finsterle et al., 2007). Only the key measurements relevant to developing the flow and transport model for the decay pipe (to be presented in Section 3) are presented in this section.

2.1 Flow Measurements

Relevant to the flow model development are (1) the measured water table level, (2) the measured rate of flow seeping from the decay tunnel walls into the drainage system, (3) the measured rate at 11 grates into the main drain, representing seepage into the walkway tunnel, and (4) the total rate of flow for the entire facility system collected at the sump.

Tables 1 and 2 list the measured and estimated flow rates in 2001 and 2002 before backfilling of the decay pipe tunnel with concrete. Measurements were taken at the target shaft pump, decay tunnel pump, target hall pump, carrier tunnel pipe, and the Minos access shaft pump, as well as the survey riser SR#2, and vent shaft EAV-1. For the decay pipe region (STA 8+48.52 to STA 30 +00), the measured flow rate varies from 165 to 304 gallons per minute (gpm). The average measured flow rate is 239.1 gpm. The last flow rate through the decay pipe region is 239 gpm measured on July 1, 2002.

The grate flow rates were also measured on May 17, 2006. The measured flow rates for the 11 grates are 2.06, 2.99, 1.53, 2.36, 0.83, 1.63, 0.44, 0.99, 0.34, 0.70, 0.10 gpm, respectively. The total measured grate flow rate is 14.07. The measured flow rates during the operation of the NuMI experiments were used to calculate the tritium mass carrying with grate flow into the main drain, and finally to the sump.

Measured total flow rates for the entire system are 322 gpm on March 12, 2002 (dry season) and 378 gpm on July 1, 2002 (wet season), including the measurements for the Minos tunnel region. The measured total flow rate decreases with time. The total flow rate measured in March 2004 is 234 gpm. Under the operation conditions, the total flow rate measured at the sump is 157 gpm and 177 gpm, respectively.

During operation of the facility, the flow rate for the decay pipe region is not measurable, because there is no access to the main rain and the dimple mat. For the modeling purpose, this flow rate is obtained through a simple linear scaling. The scaling factor of 63.2% is calculated using 239 gpm for the decay pipe and the total flow rate of 378 gpm measured on July 1, 2002. The measured total flow rate of 157 gpm is assumed to be representative of the average flow rate for the entire facility system under the operation conditions. The scaled flow rate for the decay pipe is 99.2 gpm. The average water table level of 210.30 m (690 feet) was also assumed to be representative of long-term flow conditions.

Note that there are no water saturation measurements of the concrete or geologic formation. Unsaturated conditions may have been caused by ventilation of the NuMI facility. Note that the water saturation in the decay pipe concrete is critical to the diffusion and advection of tritium generated in the backfill material. The water saturation was therefore calibrated using observations of tritium transported through the concrete to the main drain and sump.

Table 1. Measured rates of flow seeping into the excavated NuMI tunnel from different facility components in 2001 and 2002, as well as the calculated flow rates for the entire system

	Fermi Lab's GROUNDWATER INFLOW AT NuMI TUNNELS & HALLS PROJECT											
	#1	#2	#3	#4	#5	#6	#7	#8		#9	#10	#11
Location	Support Rooms	Utility Passageway	Target Shaft Pump	T. Shaft Pump Bypass to Target Hall	Target Shaft	Decay Tunnel Pump	Potable Water Inflow	Decay Tunnel		Target Hall Pump	Survey Riser 8R#3	Inflow From Construction Shaft Area to Target Hall
Measurement Method	Estimated	Estimated	Measured	Estimated	#3 - #1 - #2 + #4	Measured	Metered	#6 - #7		Measured	Estimated	Estimated
Unit	GPM	GPM	GPM	GPM	GPM	GPM	GPM	GPM		GPM	GPM	GPM
05/27/01	2	3	28	3	28	49	0	49		64	6	10
7/20/01, 10:00 pm	2	3	28	2	26	70	2.5	67		50	3	5
8/2/01, 6:00 pm	2	3	20	2	17	112	6	106		46	3	5
	#1	#2	#3	#4	#5	#6	#7	#8	#8a	#9	#10	#11
Location	Support Rooms	Utility Passageway	Target Shaft Pump	T. Shaft Pump Bypass to Target Hall	Target Shaft	Decay Tunnel Pump	Average Potable Water Inflow	Decay Tunnel to Sta 30+00	Mission Pumps	Target Hall Pump	Survey Riser 8R 3	Inflow From Construction Shaft Area to Target Hall
Measurement Method	Estimated	Estimated	Measured	Estimated	#3 - #1 - #2 + #4	Measured		#6 - #7 - #21	Estimated	Measured	Estimated	Estimated
Unit	GPM	GPM	GPM	GPM	GPM	GPM	GPM	GPM	GPM	GPM	GPM	GPM
8/21/01, 8:00 pm	2	3	21	2	18	326	37	189		45	3	5
8/22/01, 9:30 pm	2	2	20	2	18	428	46	282		42	3	5
9/18/01, 7:30 pm	1	2	0	20	17	151	21	180	75	58	3	5
9/26/01, 10:00 pm	1	2	13	6	18	375	14	281	0	51	3	5
10/1/01, 3:00 pm	1	3	3	15	14	264	1	243	0	57	3	5
1/18/02 6:00 PM	1	3	12	6	14	310	6	304	0	56	0	5
3/12/02 7:00 PM	1	3	6	4	8	190	25	165	0	35	0	1
7/1/02 6:00 PM	1	3	14	0	10	246	0	239	0	44.5	0	1

Notes: 1) On 8/21/01 and 8/22/01, the heading pumps for decay tunnel were elevated to keep rocks from damaging pumps. This flooded the face. Measurement taken while mining.

2) DT flow of 304 gpm (1/18/02) includes tunnel from Target Hall to MINOS Shaft.

3) Total flow of 422 gpm (1/18/02) includes MINOS Hall (5 gpm) and MINOS Shaft (35 gpm).

4) MINOS Access Shaft flow measured at 30 gpm. MINOS Hall estimated to be 5 gpm, and Absorber area estimated at 20 gpm. (Column # 22)

Table 2. Measured rates of flow seeping into the excavated NuMI tunnel from different facility components in 2001 and 2002, as well as the calculated flow rates for the entire system

Fermi Lab's GROUNDWATER INFLOW AT NuMI TUNNELS & HALLS PROJECT									
#12	#13	#14	#15	#16	#17	#18	#19	#20	#21
Target Hall	Carrier Tunnel Pipe	Flow Bypassing Pipe	Pre-Target Tunnel 4+47 to 5+02	Survey Riser SR#2	Vent Shaft EAV-1	Carrier Tunnel	Pre-Target Tunnel 5+02 to Const. Shaft	Construction Shaft	Total Inflow
#9 - #4 - #10 - #11	Measured	Estimated	Estimated	Measured	Measured	#13 + #14 - #15 - #16 - #17	Estimated	Estimated	#1 + #2 + #5 + #8 + #10 + #12 + #16 + #17 + #18 + #19 + #20
GPM	GPM	GPM	GPM	GPM	GPM	GPM	GPM	GPM	GPM
48	31	4	1	2	4	28	15	30	210
40	30	1	1	2	4	24	16	30	218
38	20	0	1	2	4	13	16	30	229

#12	#13	#14	#15	#16	#17	#18	#19	#20	#21	#22	#23
Target Hall	Carrier Tunnel Pipe	Flow Bypassing Pipe	Pre-Target Tunnel Sta. 4+47 to 5+02	Survey Riser SR 2	Vent Shaft EAV-1	Carrier Tunnel	Pre-Target Tunnel Sta. 5+02 to C Shaft	Construction Shaft	Vent Shafts EAV-2 / -3	Sta. 30+00 to Sta. 41+50	Total Inflow
#9 - #4 - #10 - #11	Measured	Estimated	Estimated	Measured	Measured	#13 + #14 - #15 - #16 - #17	Estimated	Estimated	Estimated	Measured	#1+2+5+8+10+12+15+17+18+
GPM	GPM	GPM	GPM	GPM	GPM	GPM	GPM	GPM	GPM	GPM	GPM
35	21	0	1	1	3	18	15	30	90	x	416
32	21	0	1	1	3	18	15	30	90	x	604
30	17	5	1	1	3	17	15	30	80	x	389
37	15	5	1	1	3	15	15	25	80	x	479
34	15	5	1	1	3	15	15	25	20	x	377
45	9	14	1	1	3	18	15	25	0	x	429
30	8	15	1	1	3	18	15	25	0	55	322
43.5	8.5	5	1	0	0	7.5	15	25	0	34	378

2.2 Concentration Measurements

Tritium concentrations in water were measured by Fermilab to understand the transport of tritium in different system components and the entire system. The data include the concentrations and flow rates representative of the entire system, the drainage system, the target pipe source area, tritium vapor, and the direct productions in concrete and interaction between tunnels and concrete (Finsterle et al., 2007). Using these data, the conceptual model of the transport mechanisms was given in the Phase I project report. Here, we focus on the tritium transport and mass balance of tritium in the decay pipe region.

For the decay pipe region, tritium is generated in the decay pipe concrete and its surrounding rocks. Tritium is transported into the walkway parallel to the decay pipe with ventilated air flow from the target hall and the absorber hall. Tritium is also transported into the decay pipe region through the main drain, and out of the region to the sump. The tritium mass in the seeping water in the walkway is transported into the main drain through 11 grates. Tritium concentrations were measured at the sump and the 11 grates, as well as the pre-grate 1 location of the main drain. However, the flow rate from the target hall through the main drain is unknown. Fermilab researchers did calculate the contributions from the grates and the pre-grate-1 main drain. They found that the majority of the tritium mass collected at the sump comes from the grates and pre-

grate-1 flow. For example, grate tritium concentrations were measured on January 30, 2007, May 10, 2007, August 17, 2007, and May 22, 2008, while the grate flow rates were measured on February 1, 2007. The contribution of tritium mass from grate flow accounts for 34%, 46%, 48%, and 69% of the total tritium mass collected at the sump, respectively. The measured sump concentration is 5.8, 8.3, 5.2, and 8.7 pCi/mL, respectively, at the 4 measurement times, while the flow rate at the sump is 163 gpm measured on February 1, 2007. By assuming zero release of tritium from the concrete and fractured rock, Hylen (2008a, b) calculated the flow rate through pre-grate 1, and found the calculated flow rate is reasonable.

The generation of tritium mass in the decay pipe concrete was calibrated using the measured tritium concentration in concrete cores in the decay pipe. However, the release of the generated tritium into the drainage system is not measured. We have to infer the release rate from the trend of tritium mass collected at the sump. The basis for the interference is that (1) the tritium mass generated in the decay pipe concrete is relativelyp large, and (2) tritium release rate increases with time, but is independent of seasons because of the unsaturated flow conditions in the decay pipe concrete. As shown in Figure 3, in the past four years of NuMI operation, the tritium concentrations in the holding tank is highly variable, with a strong correlation to the operational conditions of the system components. However, the minimum concentration stays relatively constant, indicating that the release of tritium from the concrete is constant and relatively small. The average beam intensity for the first 4 years is 1.75×10^{20} pot/year, and the average tritium concentration in the sump water is 8.0 pCi/mL. Considering the average rate of water flow into the sump is 157 gpm, the tritium mass released from the system to the sump is 2.5 Ci/year. The minimum tritium mass is less than 1.0 Ci/year.

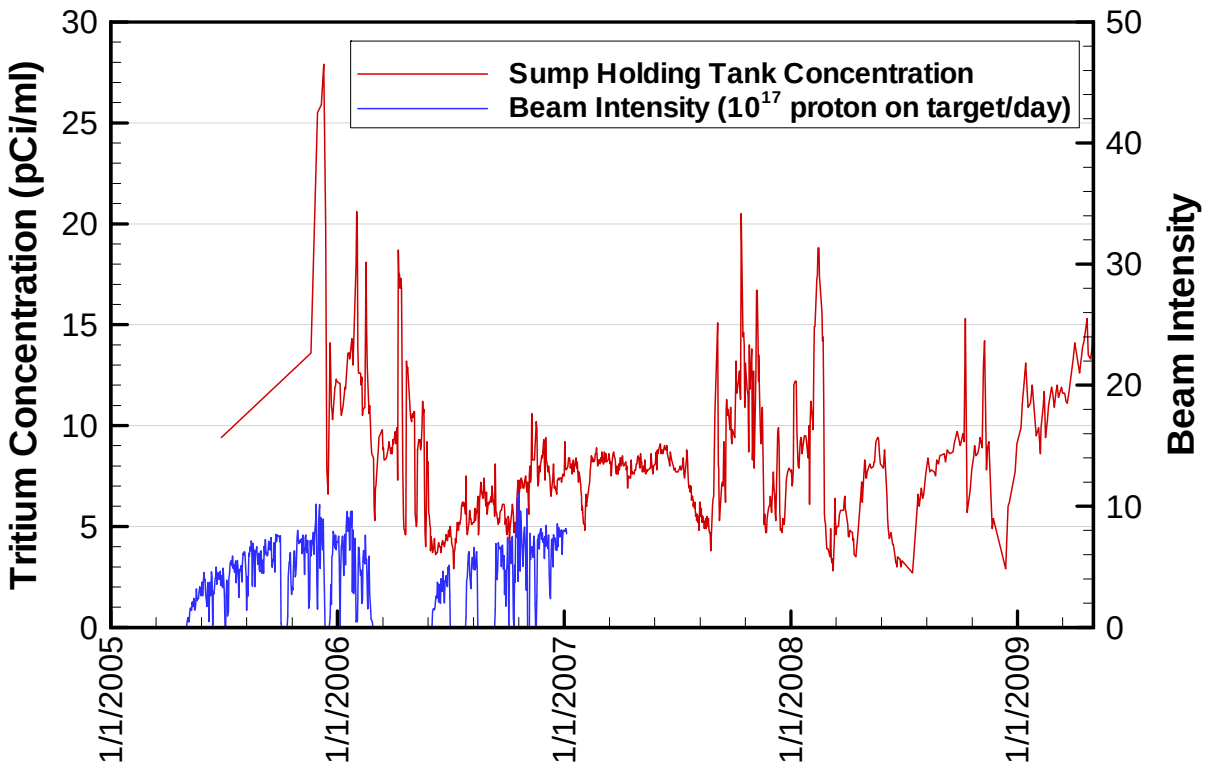

Figure 3. Tritium concentration in the sump water collected in the holding tank and beam intensity, and converted tritium mass using the flow rate of 157 gpm.

3. NUMERICAL MODEL DEVELOPMENT

To simulate the steady-state fluid flow and the tritium transport in the NuMI facility and its immediate surroundings, a three-dimensional numerical model was developed. The simulations were conducted using TOUGH2 (Pruess, 2004). Preliminary calibration was employed to estimate the rock properties and concrete water saturation using field observations of flow rates and tritium concentrations presented in Section 2 (Hylen, 2006a,b,c,d). The generation of tritium mass was modeled using the calibrated MARS model (Lundberg, 2006). Long-term tritium fate was predicted using the current and projected beam intensity of the NuMI experiments.

3.1 Model Domain

This model focused on the ~670 m long decay pipe, with 30 m by 30 m vertical cross sections centered at the vacuum pipe. The slope of the decay pipe is 5.83%. A total of 11 representative sections (labeled Section B through M) were generated. Section B was considered the base cross section; all the other sections were generated from this base cross section by shifting coordinates to account for geometric distortions, and by reassigning material types to elements. Regions assigned to a specific material type include the vacuum pipe of 0.99 m diameter, the decay-pipe tunnel, which is back-filled with concrete surrounding the vacuum pipe, the open walkway, the rock zone where tritium production is expected, and the rock zone without tritium production (see Figure 4).

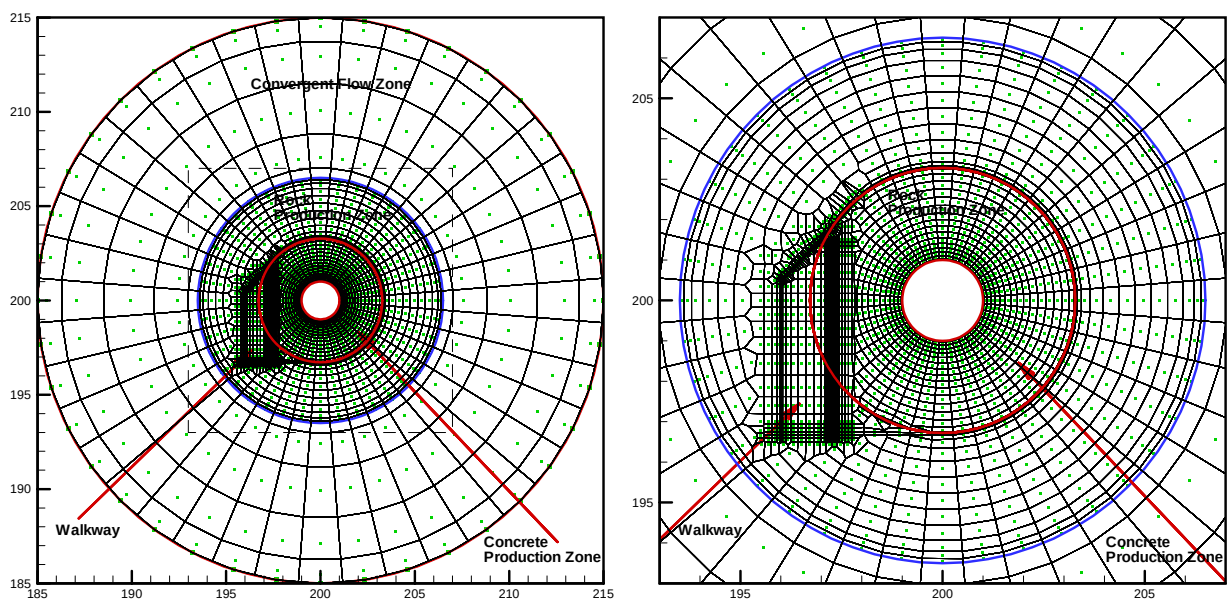

Figure 4. Base mesh at Section B: gridblock centers are shown as green dots; gridblock interfaces are in black lines. Three zones are roughly defined based on the flow conditions, materials, and underground objects: convergent flow zone (area between the outer red and blue circle), tritium production zone within rock (area between the blue and the middle red circles), decay tunnel zone backfilled with concrete (area between the two inner red circles), as well as the walkway and vacuum pipe.

3.2 Mesh Generation

As shown in Figure 4, the 2D mesh for Cross Section B (which is used as the basis for 11 representative cross sections and the 3D mesh of the decay pipe region) has different resolution for different material regions. The mesh is essentially 2D radial with different radial discretizations, from 0.01 m next to the vacuum pipe to 0.20 m at the outer radius of the concrete backfill, 0.40 m for the rock zone where tritium is produced, and 3.0 m for the tritium-free rock zone, with a smaller discretization in the transition region between different materials. In addition, the capture of water seeping into and exiting from the walkway needs a relatively high mesh resolution. As a result, the portion of the mesh representing the walkway was locally refined, with the mesh orientation aligned with the geometry of the walkway. Higher resolution was used for the rock and concrete walls to capture the sharp transition from saturated rock and from partially saturated concrete to the essentially unsaturated walkway.

To extend the generated 2D mesh for Section B to the entire decay pipe, a stream tube concept was used, i.e., the same number of gridblocks was used for each of the cross sections, and elements were connected between cross sections to form stream tubes in approximately axial direction. For each section, some of the points (i.e., intersection points of gridblock interfaces) were relocated so that the generated 2D mesh honors the geometry of the different material regions of the representative sections. As shown in Figure 5, the vacuum pipe is a rigid body with its center moving from the central line for some representative sections. The tritium-free rock zone is also a rigid body without any coordinate shift and distortion. The walkway and concrete pipe have variable geometry at different sections, so that all points within the blue circle in Figure 5 can be relocated based on the anchors. The resultant 2D cross section meshes for Sections B through M are shown in Figure 5.

Along the decay pipe, there are 49 cross sections. Their location is determined based on the location of the representative sections, the change of the section geometry between sections, and the location of 11 grates, where flow and tritium concentration measurements are available. Each section includes gridblocks of high permeability, representing the dimple mat which lies between the concrete backfill and the tritium-producing rock zone. An array of main-drain gridblocks—one for each cross section at the lowest point of the backfilled decay pipe tunnel, and connected axially to its neighboring gridblocks—was added to collect waters from the dimple mat, as well as water from the grates. For each grate, a connection was added to link the walkway floor and the main drain, representing the grates. Two gridblocks with atmospheric conditions were added to represent the EAV, and connected to the walkway gridblocks.

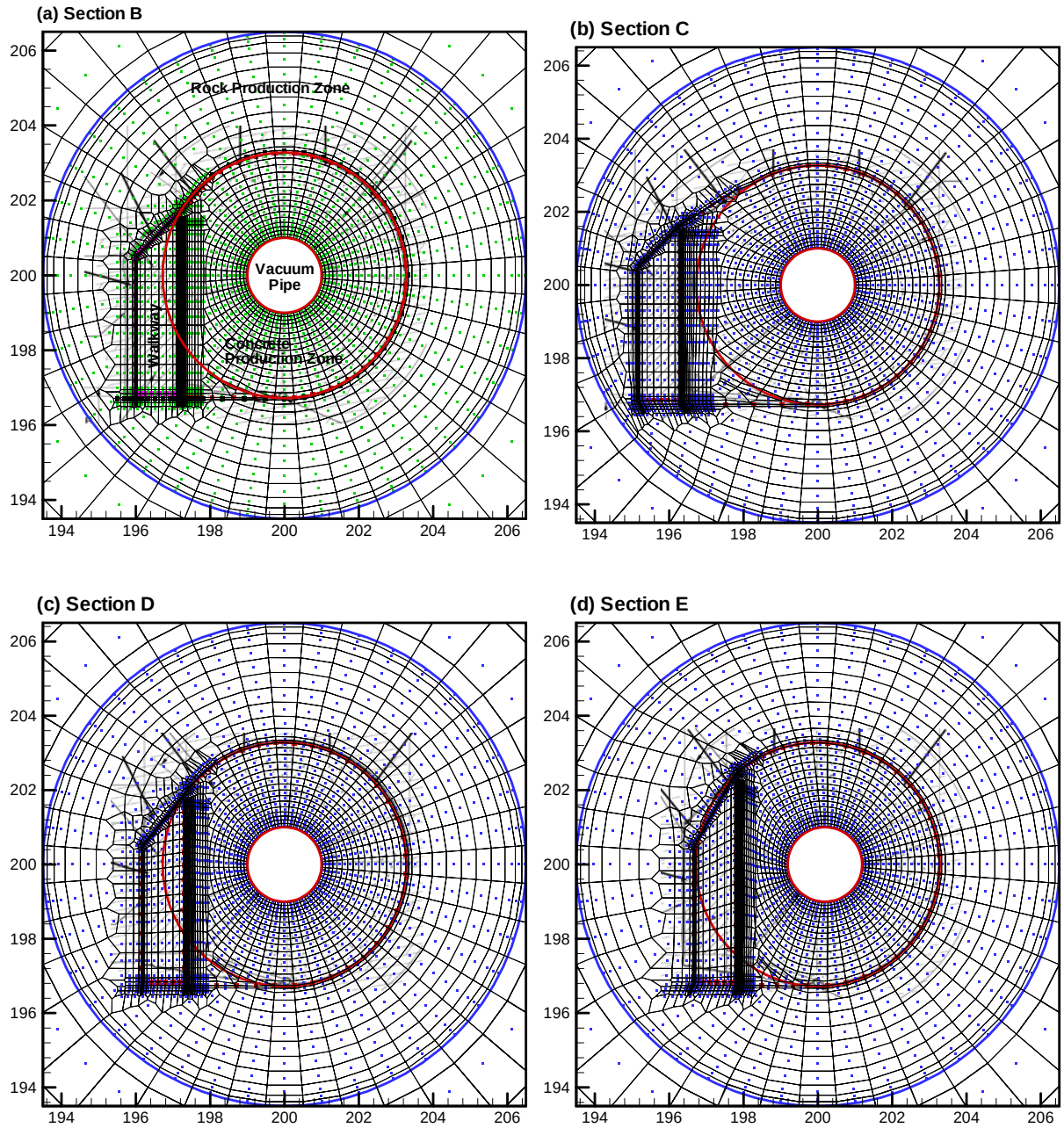

Figure 5. Representative cross sections B through M, with focus on the area for mesh deformation. The green symbols in Section B 2D mesh represent gridblocks for the base section, with gridblock interfaces in black lines. The red points (within concrete) and purple points (within walkway) are anchor points with known coordinate shifts (displacement in both X and Y directions). The interface-intersection points along the blue circle are fixed for all sections with zero shifts, while the innermost red circle (vacuum pipe) is a rigid body with horizontal shifts only. Only the portion of the mesh in the area between the blue circle and the innermost red circle is distorted.

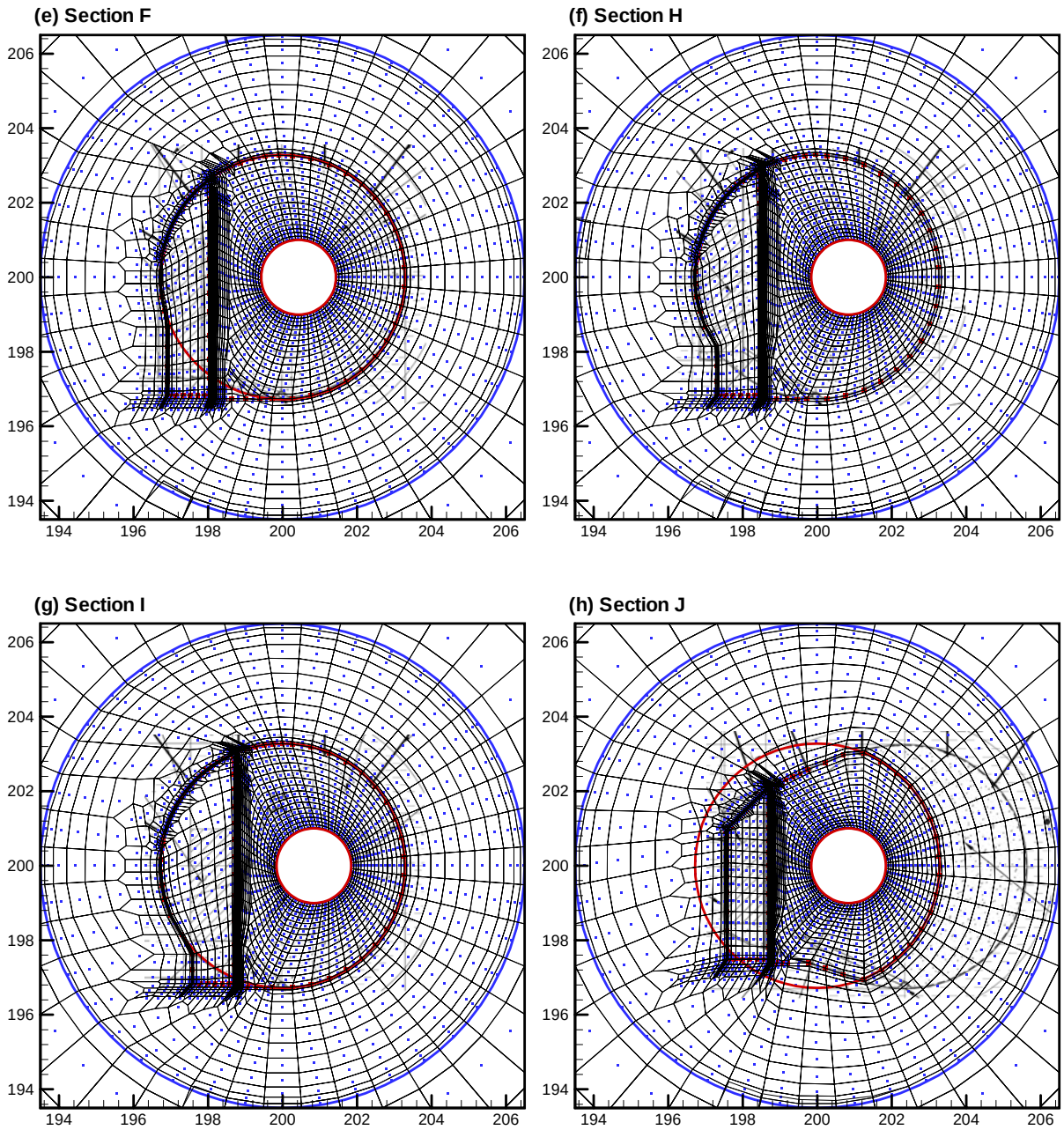

Figure 5 (cont.). Representative cross sections B through M, with focus on the area for mesh deformation. The green symbols in Section B 2D mesh represent gridblocks for the base section, with gridblock interfaces in black lines. The red points (within concrete) and purple points (within walkway) are anchor points with known coordinate shifts (displacement in both X and Y directions). The interface-intersection points along the blue circle are fixed for all sections with zero shifts, while the innermost red circle (vacuum pipe) is a rigid body with horizontal shifts only. Only the portion of the mesh in the area between the blue circle and the innermost red circle is distorted.

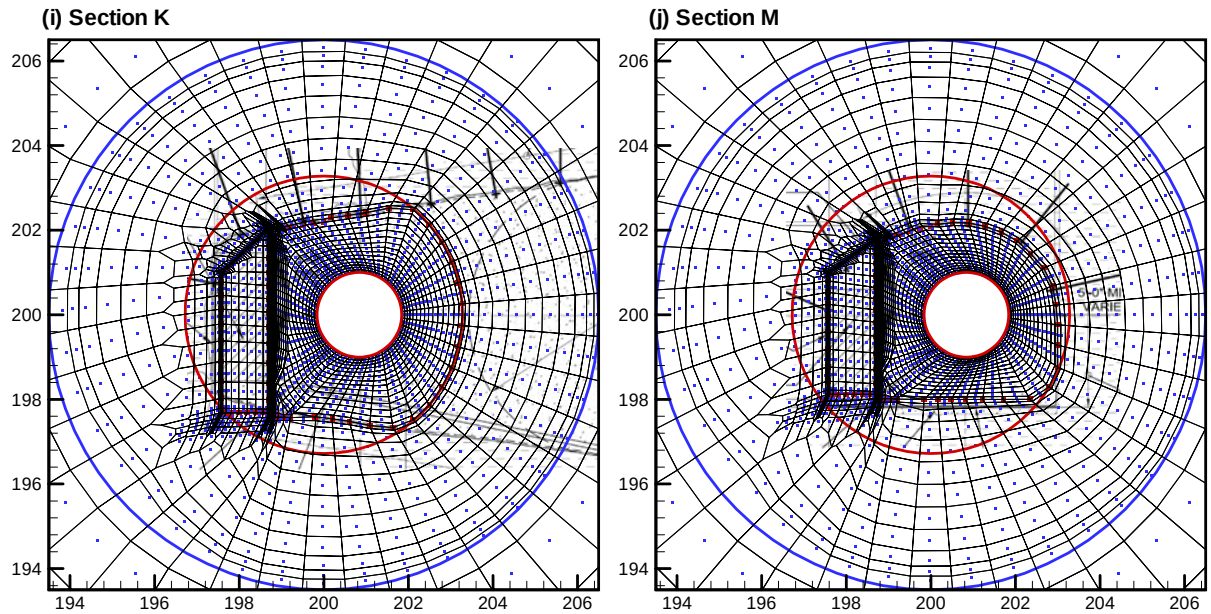

Figure 5 (cont.). Representative cross sections B through M, with focus on the area for mesh deformation. The green symbols in Section B 2D mesh represent gridblocks for the base section, with gridblock interfaces in black lines. The red points (within concrete) and purple points (within walkway) are anchor points with known coordinate shifts (displacement in both X and Y directions). The interface-intersection points along the blue circle are fixed for all sections with zero shifts, while the innermost red circle (vacuum pipe) is a rigid body with horizontal shifts only. Only the portion of the mesh in the area between the blue circle and the innermost red circle is distorted.

3.3 Material Properties

Materials for the concrete, walkway, fractured rock, dimple mat, and the drain need to be specified. The fractured rocks are located within four different rock units (from the top): Kankakee Formation (dolomite), Elwood Formation (dolomite), Maquoketa Group (shale), and shale and mudstone. Interfaces between these hydrogeologic layers are located at elevations of 199.10 m, 181.05 m, 171.60 m, and 139.00 m, respectively. The central line of the decay pipe is at 184.54 m and 145.71 m at the upstream and downstream ends, respectively. As a result, the tilted decay pipe intersects four different rock units at elevations from 199.54 m to 130.71 m.

The measured concrete permeability and porosity are 5.7×10^{-15} m^2 and 0.218, and used directly in the model. The rock properties were calibrated through steady-state flow simulation. Table 3 shows all relevant material properties and model parameters for flow and transport simulations (Finsterle et al., 2007).

Table 3**.** Hydraulic and transport parameters used in the flow and transport model

Property	**Fracture***	**Matrix***	**Concrete**
Permeability[@] Kankakee Elwood Maquoketa Shale	1.44×10^{-14} m^2 1.44×10^{-14} m^2 2.88×10^{-15} m^2 1.44×10^{-16} m^2	1.00×10^{-17} m^2	5.7×10^{-15} m^2
Porosity[#]	0.01	0.15	0.218
van Genuchten[%] α	1.0×10^{-3} Pa^{-1}	1.0×10^{-5} Pa^{-1}	1.0×10^{-3} Pa^{-1}
van Genuchten[%] m	0.6	0.6	0.6
Diffusion coefficient[^] D_m	5.0×10^{-10} m^2/s	3.0×10^{-10} m^2/s	2.2×10^{-10} m^2/s
Tortuosity[&]	0.25	0.15	0.17
Fracture spacing[$]	4 m		
Gas diffusivity	1.0×10^{-5} m^2/s		
Inverse Henry's constant[+]	3.2×10^{3} Pa		
Tritium half-life	12.3 years		

* In this study, the fractured rock is conceptualized as a dual-permeability medium. All fractures are lumped into a domain with effective continuum properties; the rock mass between the fractures is represented by the matrix continuum; both the fracture and matrix continua occupy the same computational space. Flow occurs within each of the continua as well as between the fracture and matrix continua.

@ The absolute (or intrinsic) permeability k [m^2] is a measure of the ability of a material to transmit fluid. It is related to the hydraulic conductivity K [m/s] (which is a lumped parameter that includes both material and fluid properties) by $K = k \cdot (\rho g / \mu) \approx k \cdot 10^7$. The fracture permeability is calibrated using the flow rate in the main drain; the matrix permeability is taken from Grossman (2004, Table 2); the concrete permeability is taken from Selih et al. (1996).

\# Porosity is defined as the ratio of the pore volume to total volume. Values for matrix and concrete porosities are taken from Grossman (2004, p. 6) and Selih et al. (1996), respectively Fracture porosity is defined as the volume associated with fractures per cubic meter; 1% is a typical value

% The van Genuchten model describes the capillary pressure and relative permeability as a function of liquid saturation (van Genuchten, 1980). The capillary pressure P_c [Pa] is the difference in pressure across the interface of two immiscible fluids; it can be expressed as a macroscopic quantity and related to the average saturation within a continuum element. Relative permeability k_{rl} [-] captures phase interference processes, i.e., the reduction in permeability of a given phase due to the presence of another phase. Both quantities depend on fluid properties as well as the pore size distribution and pore connectivity. The parameter α is related to the air-entry pressure (the threshold pressure that has to be overcome for gas to be able to displace liquid—it is determined by the largest pore); the parameter m is related to the pore-size distribution. At the NuMI facility, two-phase conditions may arise due to drainage and ventilation effects.

^ Defined as $D_m = \tau \cdot D_0$, where d0 = 2.0×10^{-9}m^2/s; see Finsterle et al. (2007)

& Tortuosity is defined as the ratio of the distance between the two end points of a pore segment and the actual length of the tortuous pore. The tortuosity of the straight pore is 1; the tortuosity of a twisted pore approaches zero. Under two-phase conditions, the tortuosity is saturation-dependent. Tortuosity is used here to calculate diffusive fluxes in a porous medium given the diffusivity in free water. The concrete tortuosity is estimated from the diffusion-cell experiments described in Section 5.3; fracture and matrix tortuosities represent typical values.

$ Based on Grossman (2004, Table 5)

\+ Partitioning of tritium between the liquid and vapor phase is approximated here using an inverse Henry's constant, which can be thought of as an aqueous phase solubility of the radionuclide.

3.4 Initial and Boundary Conditions

The initial pressure distribution was obtained by running the model to steady state using the following boundary conditions. First, the hydrostatic pressure for the gridblocks of the 3D mesh was calculated using their *Z*-coordinates and accounting for the fact that the water table is at an elevation of 210.30 m (690 feet). This calculated pressure was fixed at the outer boundary gridblocks of the model domain along all faces that are parallel to the decay pipe axis. No-flow boundaries were specified at the two faces perpendicular to the axis, i.e., at Sections B and M. Convergent flow is induced from the outer boundary to the dimple mat and the main drain, which—at its lowest point—is held at atmospheric conditions. The two EAV gridblocks are at atmospheric pressure. For transport simulations, the tritium generation rate was calculated using the calibrated MARS model; only the tritium generated in the decay pipe concrete region is considered in the simulations. Since the outer boundary is far away from the tritium-containing region, this boundary has a tritium concentration of zero. Upstream and downstream boundaries are impervious to tritium transport, except the downstream main drain, where an outflow boundary condition was used.

3.5 Steady-State Simulation and Comparison to Flow Data

The permeability of the four rock units was adjusted to match the total flow rate measured for the decay pipe, as well as the measured flow rate through the grates. The calibrated total flow rate is 85.6 gpm for the entire decay pipe, with 59.6 gpm through the dimple mat and 26.0 gpm through the grates. The total simulated flow rate is smaller than the estimated of the actual rate of 99.2 pgm (inferred from the measured rate and scaled as described in Section 2), while the calibrated grate flow rate is higher than the measured rate of 14.1 gpm. Considering the large uncertainties in the scaling of the total sump rate, the calibrated rates are considered reasonable. The calibrated permeability for the four rock units are 1.44×10^{-14}, 1.44×10^{-14}, 2.88×10^{-15}, 1.44×10^{-16} m^2 for the Kankakee Formation, the Elwood Formation, the Maquoketa Group of Shale, and the Shale/Mudstone. The total flow is insensitive to the flow across the concrete; consequently, the measured concrete permeability (and porosity) values are used directly.

Note that the convergent flow through the outer boundary to the main drain is through the dimple mat of high permeability and through water seeping from the ceiling and walls of the walkway to the walkway floor, entering the grates and discharging to the main drain.

The amount of water entering the concrete from the rock (i.e., the connection between the dimple mat and the concrete) and flowing through the partially saturated concrete to the lower section of the backfilled tunnel and into the main drain is the key factor affecting advective transport of tritium generated within the concrete. The advective transport from the high-concentration area close to the vacuum pipe to the main drain depends on concrete permeability and water saturation. Unlike the convergent flow through the fractured rock to the main drain, the change of the concrete saturation from its initial condition after the excavation is believed to be slow, depending on the connection between the concrete and dimple mat, as well as the capillarity of the concrete.

Since there are no saturation measurements, the water saturation of the concrete was calibrated by comparing the measured tritium concentrations in the holding tank to the simulated concentration in the downstream main drain gridblock. Advective transport of tritium is very

sensitive to the effective permeability, i.e., the product of intrinsic permeability and water relative permeability, which is a function of water saturation.

A sensitivity analysis of concrete intrinsic permeability was conducted by simulating the steady-state flow and tritium transport. The intrinsic permeability was varied from the measured 5.7×10^{-15} m^2 to 5.7×10^{-18} m^2. The beam intensity was assumed to 1.5×10^{20} pot/year, and the total tritium generated in 10 years was 57.1 Ci. Figure 6a shows that the tritium mass remaining in the concrete at the end of 10 years strongly depends on the intrinsic permeability of the concrete. For example, for an effective permeability of 5.7×10^{-15} m^2 with a saturation value close to one, almost all tritium was flushed out by advective transport to the main drain. This indicates that, on average, more than 4.0 Ci are released annually from the concrete, which is contrary to the observation of less than 1.0 Ci/year at some times for the combined contributions of all tritium sources.

A further sensitivity analysis was conducted for concrete water saturation. The water saturation was calibrated using the 4-year operational data. A constant rate of 1.75×10^{20} protons on target per year was assumed. The total generation rate of tritium in both concrete grains and pores is r = 30.57 Ci/year for fully saturated conditions, assuming that cross sections for tritium generation in water and the solid phase are approximately the same, and tritium generation in pore air is negligible. For unsaturated concrete, the total tritium mass equals to $r\{(1-\varphi)+S\varphi\}$, where S is the water saturation of the concrete and φ is the concrete porosity. The tritium mass generated in the pore water amounts to $6.66 \cdot S$ Ci/year. The total tritium mass for the 4 years of operation is $26.65 \cdot S$ Ci.

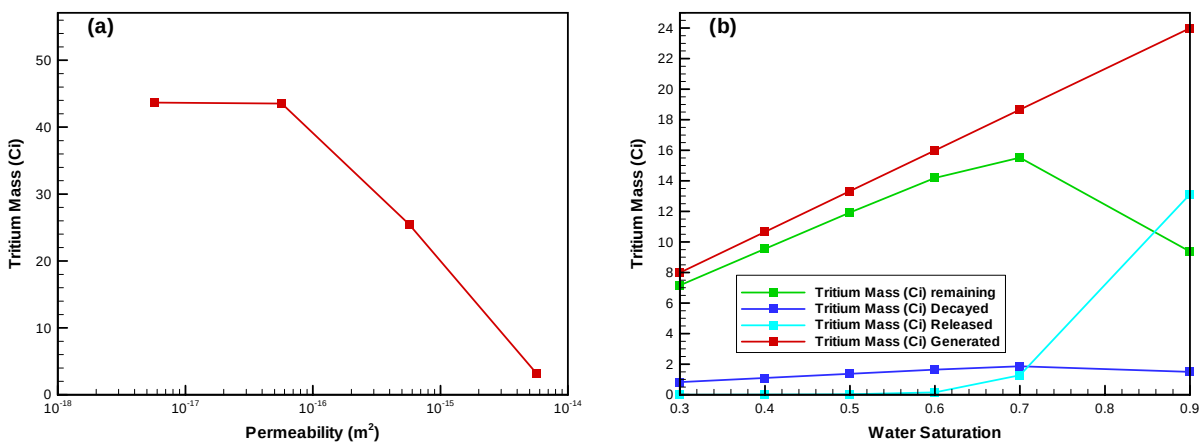

Figure 6. Tritium mass remaining in the concrete as a function of (a) intrinsic permeability with high water saturation, and (b) water saturation with the measured intrinsic permeability of concrete. Also shown in (b) are saturation-dependent tritium mass generated and decayed in concrete pore water, as well as the mass released from concrete pore water to the drainage system.

Figure 6b shows the mass balance of the generated tritium mass during the 4-year facility operation. The total tritium mass increases with water saturation from 8.0 Ci for $S = 0.3$ to 24.0 Ci for $S = 0.9$. Most of the generated tritium mass remains in the concrete pore water except at a high saturation of 0.9, where it is washed out advectively. The tritium mass that decayed within the concrete is between 0.83 Ci at $S = 0.3$ and 1.87 Ci at $S = 0.7$. Most importantly, the tritium mass released into the drainage system from concrete pore water remains negligible at low saturations. With saturation as high as $S = 0.7$, the total released tritium increases to 1.28 Ci for the 4 years of operation.

The analysis of concentration data described in Section 2 suggests that the tritium collected in the main sump has negligible contributions from the decay pipe concrete. As shown in Figure 6b, tritium releases from the concrete to the main drain reach insignificant levels if the concrete is assumed unsaturated. For the assumed absolute permeability and relative permeability function, tritium release essentially ceases for saturations lower than about 0.5.

The inferred low water saturation in the concrete pipe indicates that the connection between fractured rock and the concrete pipe through the dimple mat is negligible, so that water does not easily enter the concrete through gravitational or capillary imbibition. If the concrete is assumed to be almost saturated during the first year of operation in 2006, approximately 5.0 Ci of generated tritium is predicted to be released into the main drain from the concrete alone. In contrast, the average tritium mass collected in the holding tank is 2.5 Ci per year in the first 4 years of beam operation. This amount includes contributions from all tritium sources, specifically tritium migrating along the passageway, which is considered a major contributor, whereas the contribution from the concrete during the early stages of beam operation are expected to be very small, as discussed in Section 2. Given that the predicted tritium release from the concrete is twice as high as the observed tritium from all sources, and is thus significantly higher than the expected contribution from the concrete, it is unreasonable to assume that tritium generated in the concrete is highly mobile. Considering the observed minor contribution of the tritium in the concrete to the tritium mass collected in the holding tank, and honoring the measured concrete permeability and for the assumed relative permeability function, the water saturation in the concrete pipe is expected to be around 0.5.

It is believed that the calibrated water saturation and simulated tritium migration are reasonable and consistent with the relatively small amount of tritium released from the decay pipe concrete during the initial four years of beam operation.

3.6 Tritium Transport Simulation and Prediction

The calibrated hydraulic properties of the fractured rock and the calibrated water saturation in the concrete pipe were used to simulate the steady-state flow field, which provides the basis for the subsequent tritium transport simulation. The beam intensity was given by Fermilab for current and future conditions. As shown in Figure 7, the NuMI experiments are conducted at relatively low energies from 2006 to 2013, followed by six year of medium-energy experiments from 2014 to 2020. At that point, beam operation is stopped. The MARS model results were used to calculate the tritium mass generation rates in the concrete for both low- and medium-energy conditions. It was assumed that the generation rate is the same for the solid concrete and pore water under fully saturated conditions. Very minor tritium generation in the air present in the pores of the unsaturated concrete is neglected.

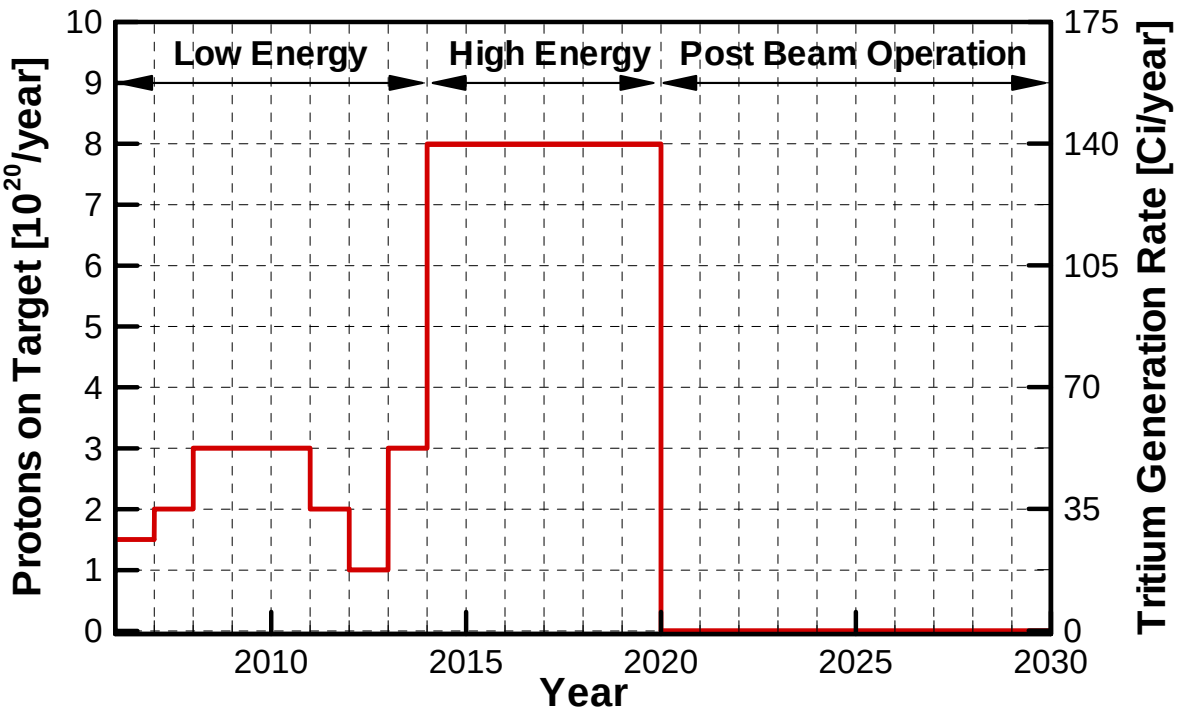

Figure 7. Beam intensity (POT/year) for the low-energy experiments from 2006 to 2013 and the high-energy experiments from 2014 to 2020. The corresponding tritium generation rates in the concrete assume fully water saturated conditions.

Figure 8 shows the tritium mass generated in pore water as a function of time. The total tritium mass generated for the 14 years of experiments is 126.65 Ci. Note that the water saturation is 0.5 and the concrete porosity is 0.218. The generated tritium mass in concrete solids of 908.53 Ci is assumed to be immobile. This assumption underestimates the amount of tritium being released to the main drain, as part of the tritium generated in the concrete may diffuse to the grain surface by solid diffusion, recombine, and desorb, making it available for advective and diffusive transport in the pore water. Recall, however, that the overall release of tritium from the decay pipe concrete to the main drain is very small.

The transport simulation was conducted for the tritium generated in pore water only. The tritium mass remaining in the concrete pore water reaches its maximum of 96.7 Ci after 14 years of beam operation. After beam operation and tritium generation stops, the tritium inventory in the concrete declines by 2030 to 50.6 Ci, which is about half of its peak value at 2020. This reduction is mainly due to radioactive decay (about 40 Ci). A smaller contribution has been flushed out of the concrete and collected in the main drain leading to the sump. The total tritium mass released into the drainage system is about 6.7 Ci (note that this is a cumulative release rate, i.e., the decay of tritium once it enters the sump is not factored in). Note that tritium release rates keep increasing during the 10 years from 2020 to 2030 despite the absence of new tritium generation and reducing tritium inventory in the concrete. This continued, increased release is the delayed response to the high-energy beam-operation period. The release rate is expected to reach its maximum shortly after 2030. Nevertheless, the release of tritium into the drainage system is relatively small, only about 5% of the total amount of tritium generated in the concrete pore water, indicating that tritium is well contained during the 14 years of experiments, and is only slowly released afterwards such that most of the inventory will decay within the concrete rather than in the drainage system or natural environment. This containment of generated tritium in concrete can be attributed to (1) low water saturation and the correspondingly low mass generation in potentially mobile pore water, (2) low advective transport caused by the small relative permeability, and (3) low effective diffusion coefficient, which depends on water saturation.

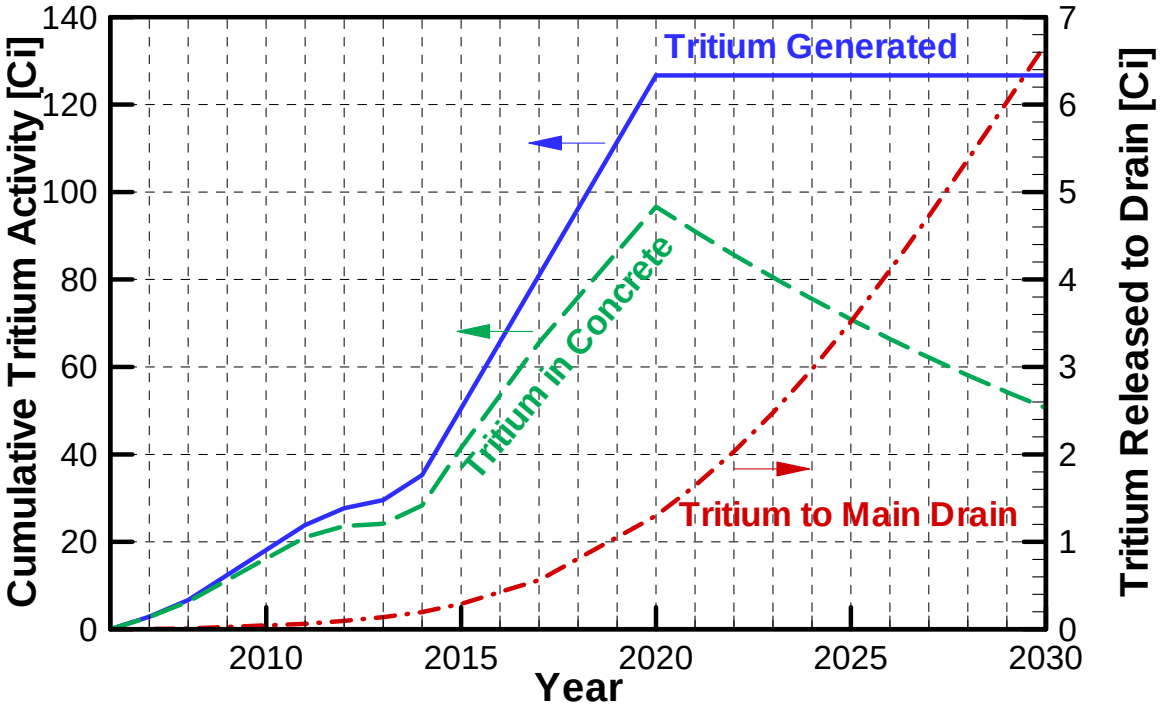

Figure 8. Cumulative activity of tritium generated and contained in the concrete pore water, and released into the drainage system during and after beam operation.

4. SUMMARY AND CONCLUSIONS

To simulate the variably saturated flow and tritium transport in the NuMI facility, a three-dimensional numerical model was developed and calibrated. This model focused on the 670 m long decay pipe and the long-term fate of tritium generated by the physical experiments. This model honors the changes in the geometry of the components (backfilled decay pipe tunnel, walkway, vacuum pipe, and fractured rock) of the decay pipe along its axis. A three-dimensional computational mesh was generated using mesh deformation to account for the geometric changes.

A steady-state flow model was developed to simulate the variably saturated flow for the decay pipe region and its surrounding fractured rock. The model was calibrated using the total flow rate measured at the sump and the total grate flow at the 11 grates. The calibrated fractured rock permeabilities provide a reasonable match between the simulated and measured flow rates. The concrete effective permeability (i.e., relative permeability at reduced water saturation with known measured concrete permeability) was calibrated using the following observation: the total tritium mass collected at the sump is mainly from global air flow and tritium mass transfer between tritium-containing air and seeping water along tunnel walls. The calibrated water saturation of 0.5 provides a simulated tritium release from the decay pipe concrete that is negligible in comparison to the tritium mass collected at the sump.

Based on the calibrated flow field and the measured concrete diffusion coefficient of tritium, the long-term fate of tritium generated in the concrete under the projected beam intensity was predicted. The tritium generation in the concrete pore water (as well as in the concrete solids) was simulated using the calibrated MARS model. The time-dependent beam intensity and tritium generation rate was used for the prediction. More tritium mass is generated during the last 6 years of medium-energy experiments than the first 8 years of low-energy experiments. Within the 14-year experiments, 1.7% of the total generated tritium mass in concrete pore water is released to the drainage system. 76.3% of the generated tritium remains in the concrete, while 22.0% of the generated tritium is decayed.

The relatively small release of tritium into the drainage system may be attributed to (1) reduced tritium generation in only partially water saturated concrete pores, (2) small advective tritium transport, caused by the low saturation of concrete, and (3) small diffusive transport, caused by the low effective diffusion coefficient in the unsaturated concrete. The last two conditions for tritium containment during the experiments may become less effective after the underground NuMI facility is decommissioned and flooded.

5. ACKNOWLEDGMENT

We would like to thank Fermilab staff for providing data and for most useful discussions. This work was supported by the Fermi National Accelerator Laboratory (Fermilab). The support is provided to Berkeley Lab through the U.S. Department of Energy Contract No. DE-AC02-05CH11231.

6. REFERENCES

Finsterle, S., M. Conrad, B.M. Kennedy, K. Pruess, T. Kneafsey, R. Salve, G. Su., and Q. Zhang, *Mobility of Tritium in Engineered and Earth Materials at the NuMI Facility, Fermilab*, Report LBNL-61798, Lawrence Berkeley National Laboratory, Berkeley, Calif., March 2007.

Hylen, J., NuMI tritium sources, models, Powerpoint presentation, April 18, 2006a.

Hylen, J., Projects Document 144-v1 CHAFT tritium humidity transport model, Fermi National Accelerator Laboratory, October 2006b.

Hylen, J., Projects Document 102-v3, Tritium-time-ordered-spreadsheet, Fermi National Accelerator Laboratory, December 2006c.

Hylen, J., Projects Document 152-v1,core samples spreadsheet, Fermi National Accelerator Laboratory, December 2006d.

Hylen, J., Chaft Model Spreadsheet , Projects Document 8-v1, Fermi National Accelerator Laboratory, December 2006e.

Hylen, J., email communication entitled "water flow from target hall", October 8, 2008a.

Hylen J., Projects Document DOCDB-374. , Fermi National Accelerator Laboratory, 2008b.

Lundberg, B., Tritiated water in the decay region: model comparisons to data, Projects Document 136-v3, , Fermilab Report, December 2006.

Pruess, K, The TOUGH Codes—A family of simulation tools for multiphase flow and transport processes in permeable media, *Vadose Zone J*., 3, 738–746, 2004.

Genuchten, M.T., A closed-form equation for predicting the hydraulic conductivity of unsaturated soils, *Soil Sci. Soc. Am. J.*, *44*, 892–898, 1980.